Crystallized V2O5 as oxidized phase for unexpected multicolor electrochromism in V2O3 thick film

Issam Mjejri, Manuel Gaudon, Giljoo Song, Christine Labrugère, Aline Rougier

Crystallized V_2O_5 as Oxidized Phase for Unexpected Multi-Color Electrochromism in V_2O_3 thick film

Issam Mjejri[†‡], Manuel Gaudon[†‡], Giljoo Song[†‡], Christine Labrugère[^] and Aline Rougier[†‡]*

[†]CNRS, ICMCB, UMR 5026, F-33600 Pessac, France
[‡]Univ. Bordeaux, ICMCB, UMR 5026, F-33600 Pessac, France
^CNRS, Université de Bordeaux, PLACAMAT UMS 3626, F-33600 Pessac, France

*Corresponding Author: aline.rougier@icmcb.cnrs.fr, ICMCB-CNRS, 87 avenue du Dr Albert Schweitzer, 33608 Pessac cedex, France

KEYWORDS. Electrochromism materials; Vanadium oxides; Polyol synthesis; Doctor Blade; Optical properties

ABSTRACT: Our e-connected society is eager to develop devices with tunable colors. Electrochromic materials, able to modify their optical properties under an applied voltage, offer a smart solution. In the present study, we have successfully synthesized two vanadium oxide powders from a polyol mediated synthesis and powder suspensions were coated on glass/ITO substrates by doctor blading. The electrochemical and optical properties of the V_xO_y films are investigated by cyclic voltammetry (CV) coupled with *in-situ* UV–Visible spectroscopy. Both V_2O_5 and V_2O_3 films exhibit reasonably good cycling stability, significant reflectance modulation, high optical contrast and good memory effects revealing the unknown EC properties of V_2O_3. The similar green ⇄ blue ⇄ orange reversible color changes for both vanadium oxides appears suitable for display application. Then, the evolution of the vanadium cation oxidation states and of the structure of V_2O_5 and V_2O_3 upon cycling are analyzed by *ex-situ* XPS and *ex-situ* XRD (at grazing incident angle). This work highlights a robust and novel scenario upon cycling, nearly the same whatever the raw film composition that shows, for each cycle, the crystallization of V_2O_5 upon oxidation, followed by amorphization upon reduction.

I. INTRODUCTION

With the rapid development of clean renewable energy and increasing demands for multi-electrochromic devices, tremendous efforts have been pursued to find alternative materials that modulate several colors depending on redox potential with high performances and low cost.[1-5] For many years electrochromic (EC) materials have been of great academic and commercial interest and recognized as one of the key "green" technologies for sustainability and energy savings in building environments.[6, 7]

Over the past decades, tungsten oxide (WO_3), that switches to blue upon reduction, has been extensively studied due to its outstanding electrochromic properties.[8-10] It is currently used in most of the commercial applications based on the modulation of transmittance including in particular smart windows. Aiming at enlarging the range of available colors well suitable for displays applications, intensive researches have been focusing on alternative materials, including polymers [11] or more recently Metal Organic Framework.[12] In the oxide family, V_2O_5 has come up as a promising electrochromic material for device application because of its multi-color reported in various electrolytes.[13-17] Besides, its abundance and layered structure facilitate the exchange of large amount of Li cations.[18-20]

Vanadium cation exists in V^{2+}, V^{3+}, V^{4+} and V^{5+} states in vanadium oxide compounds that are categorized as single and mixed oxides based on Magneli (V_nO_{2n-1}) and Wadsley ($V_{2n}O_{5n-2}$) series.[21] Indeed, the multivalent nature of vanadium cation associated with distinct colors earns it the name of the Norse Goddess of beauty, Vanadis. Meanwhile, the coexistence of various oxidation numbers offers a drastic challenge to prepare with a stoichiometric target only one single phase, especially as vanadium oxide thin or thick films. The uses of vanadium dioxide: VO_2 and vanadium sesquioxide: V_2O_3 are more popular than other V_xO_y forms due to their unique reversible metal-insulator phase transition (MIT). [22, 23] V_2O_3 phase is known for its phase transition coupled with a magnetic disordering versus temperature. [23, 24] In this work, it will be shown that, next to the magnetic properties, the V_2O_3 phase is characterized by unexpected electrochromic properties further proving the high diversity of the physico-chemical properties of vanadium oxides. On the contrary, due to its stability and great properties, V_2O_5 has been mentioned many times in literature as positive electrode for lithium/sodium batteries or optical batteries (electrochromic device). However, despite the diversity of papers, dealing with the electrochromic properties of V_2O_5 films, explanations on the observed preferential crystallographic orientation and the origin of the color changes remain a subject of debate.[25] Besides, V_2O_5 is one of the only materials that clearly shows both anodic and cathodic colorations as a result of the occurrence of various oxidation states associated with different colors.[26] Indeed, depending on the vanadium oxidation number, V_2O_5 based electrochromic films exhibit several colors, thus offering the possibility of obtaining multicolor displays.

Several synthetic ways such as microemulsion-mediated systems, arc discharge, laser-assisted catalysis growth, solution, vapor transport, and solvothermal and hydrothermal methods have been successfully explored to fabricate various kinds of nanostructured vanadium oxides and their derived compounds.[27-29] In this paper, we use a simple method for the synthesis of various submicronic particles vanadium oxides with valence state controlled.

The electrochromic performance of vanadium oxide depends on several parameters including film thickness, morphology and porosity and the deposition method. Various physical and chemical techniques such as, thermal evaporation, electron beam evaporation, magnetron sputtering, sol-gel, electrochemical deposition and pulsed laser ablation have been used for the deposition of vanadium oxide films.[30-32] Among several deposition techniques, Doctor Blading presents the advantage of high versatility, low cost, reasonable deposition rates and simplicity in experimental parameters modulation.

In this work, based on our recent study,[33] we report a robust synthetic methodology that provides access to stoichiometry-control of the final films (V_2O_5 or V_2O_3). The polyol route used to synthesize the pure vanadium oxides is low cost and easy transferable in large scale production.

In a second part, the electrochromic properties of the Doctor Blading V_2O_3 and V_2O_5 thick films are characterized by cyclic voltammetry in ionic liquid combined with *in-situ* optical measurements and *ex-situ* XRD after cycling, and compared. Several redox steps are observed and discussed, which gives rise to a variety of color transitions as a function of the applied voltage. Moreover, the optical properties of the vanadium oxide films assigned to the different oxidation-reduction steps upon electrochemical cycling are characterized by *ex-situ* X-ray photoelectron spectroscopy measurements.

Finally, consisting of the main discovery issued from these studies, the very surprising similarities of the electrochromic behaviors of V_2O_3 and V_2O_5 raw films will be analyzed and deeply discussed thanks to grazing incidence X-ray diffraction.

II. RESULTS AND DISCUSSION

II.1. Characterization of V_2O_3 and V_2O_5 powders

The XRD patterns of the V_2O_3 and V_2O_5 powders synthesized by the polyol process as described in the experimental section (IV) and supporting information, are shown in **Figure 1**. It is obvious that the crystalline phases for vanadium oxides are discriminatory depending on the gas nature used in the thermal treatment, either Ar/H_2 for V_2O_3 or air for V_2O_5. No secondary phases are found in these patterns, and the sharpness of the diffraction peaks highlights the highly crystalline nature of the powders. Indeed, the diffraction pattern of the powder annealed under 95% Ar/5% H_2 gas mixture (**Figure 1a**), shows the presence of narrow peaks, suggesting a material with high crystallinity. The d-spacing values of all diffraction peaks are identical to those of the rhombohedral crystalline phase V_2O_3 with (00-034-0187 JCPDS data file; R-3c space group). No peak of any other phase or impurity was detected from the XRD pattern indicating that V_2O_3 with high purity can be synthesized via polyol synthesis at 160 °C for 1 h followed by an annealing at 500 °C under 95% Ar/5% H_2 gas mixture.

The X-ray pattern of the powder annealed under air (**Figure 1b**) shows that all the peaks are perfectly indexed to the orthorhombic V_2O_5 with Pmmn space group. All of the isolated phases are well-crystallized; nevertheless, despite the same temperatures and dwell times used for the annealing, the peak widths vary with the vanadium oxidation state: they increase as the valence state decreases.

To complete the structural studies, refinements using two models are compared: full-pattern matching using an isotropic peak profile function (Caglioti function) and full-pattern matching using an anisotropic peak profile function with a crystallographic direction corresponding to the (110) axis for both compounds. By comparison of the results obtained with the two full-pattern matching, the crystallite shapes are clearly anisotropic with an elongation along the (110) crystallographic axis. The use of an anisotropic model allows a significant decrease of the reliability factors R_p, R_{wp}, and R_{exp}. The unit cells and reliability factors of the anisotropic refinement for V_2O_3 and V_2O_5 are gathered in **Table 1**.

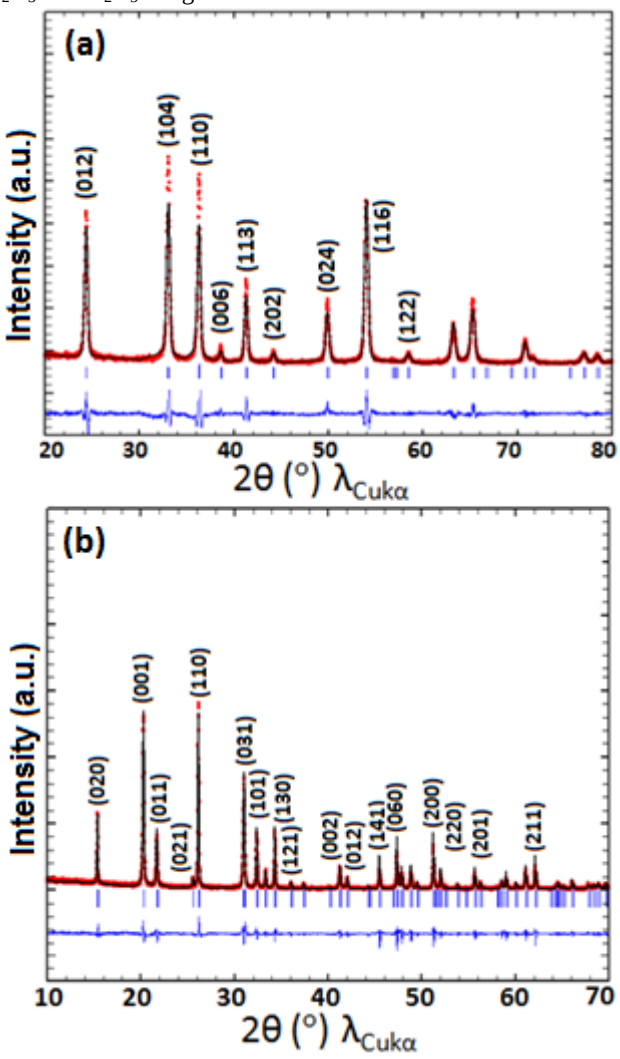

FIGURE 1. Full-pattern matching using an anisotropic peak profile of V_2O_3 (vanadium sesquioxide; $R\bar{3}c$ space group) powders (a) and V_2O_5 (vanadium pentoxide; Pmmn space group) powders (b).

TABLE 1. Unit-cells parameters and R reliability factors extracted from the pattern matching refinement of V_2O_3 and V_2O_5 powders.

	***a* (Å)**	***b* (Å)**	***c* (Å)**	***R* factors**

V_2O_3	4.9517(3)	= *a*	13.999(1)	R_p = 14.2 R_{wp} = 19.8 R_{exp} = 10.4
V_2O_5	11.5110(1)	3.5640(2)	4.3723(5)	R_p = 14.6 R_{wp} = 19.9 R_{exp} = 10.7

SEM images show a drastic evolution of the morphology from the as-synthesized V_2O_3 to V_2O_5 powders while both consist of homogeneous particles (**Figure 2**). Quasi-spherical agglomerates with individual size of about 100 nm diameter are visible.

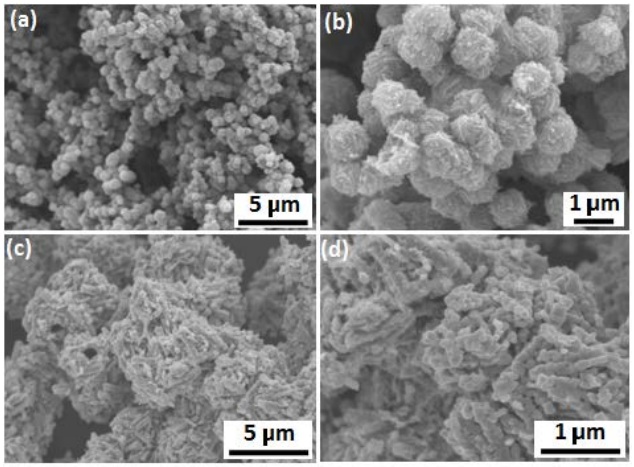

FIGURE 2. SEM Images of V_2O_3 (a, b) and V_2O_5 (c, d) powders.

The TEM images (**Figure 3**) show that the oxides consist of submicronic crystallites aggregated in packs. In good agreement with the narrower diffraction peak widths (**Figure 1b**), the V_2O_5 crystallites exhibit larger diameter. The average crystallite diameter can be roughly estimated as ∼100−150 nm for V_2O_5 and decreases to about 30 nm for V_2O_3.

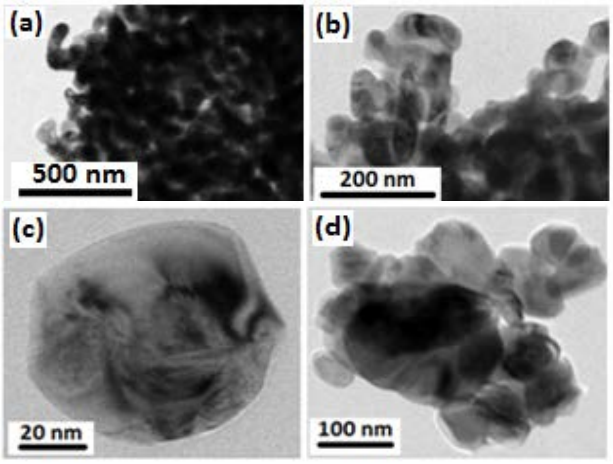

FIGURE 3. TEM Images of V_2O_3 (a, b) and V_2O_5 (c, d) powders.

II.2. From V_2O_3 and V_2O_5 powders to thick films

The SEM top-surface images of V_2O_3 and V_2O_5 films are reported in **Figure 4a and 4b**, respectively. The morphology of the V_2O_3 film is homogeneous, without any large aggregates or agglomerates. The XRD pattern of the as deposited V_2O_3 film is similar to the one of the powder **(Figure S1)**; thus the crystallite size and shape of the V_2O_3 powder appear not modified by the film deposition Doctor Blading process. To support this assertion, it can be added that the X-ray diffraction pattern of the V_2O_3 film can be refined using an isotropic peak profile function, leading to roughly the same parameters and peak profile as for the starting powder. On the contrary, a drastic evolution of the morphology from powder to film is observed for V_2O_5. It is obvious that the deposition method plays an important role in modifying the surface morphology of the vanadium oxide films. Indeed, the V_2O_5 film consists of platelets arranged parallel to the substrate (**Figure 4b**). For the V_2O_5 film, the X-ray diffraction pattern (**Figure 4c**) reveals that the d-spacing values of the diffraction peaks match with the ones of the orthorhombic crystalline phase and the ones of the ITO sub-coating. A clear preferential orientation is shown. Indeed, the main peaks located at 2θ = 20.2° and 40.0° corresponding to the (001) and (002) miller indexes, are of very large intensity, which indicates that the a-b plane of the film is parallel to the substrate (i.e. with c-axis as preferential orientation). From the X-ray pattern refinement using anisotropic peak profile function, the crystallite sizes along (001) and (hk0) directions are calculated of about 1.2 µm and 20 nm, respectively. The remarkable anisotropy of the V_2O_5 film's crystallites, may be due to surface dissolution–recrystallization of the crystallites into the suspension before the Doctor-Blade coating. A phenomenon of surface dissolution–recrystallisation of the V_2O_5 particles into the as-prepared inks for deposition involves that a change of stoichiometry between vanadium and oxygen must not be excluded, especially near the particles' surface.

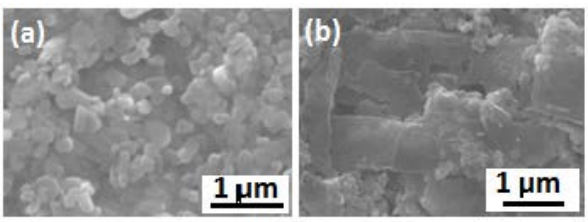

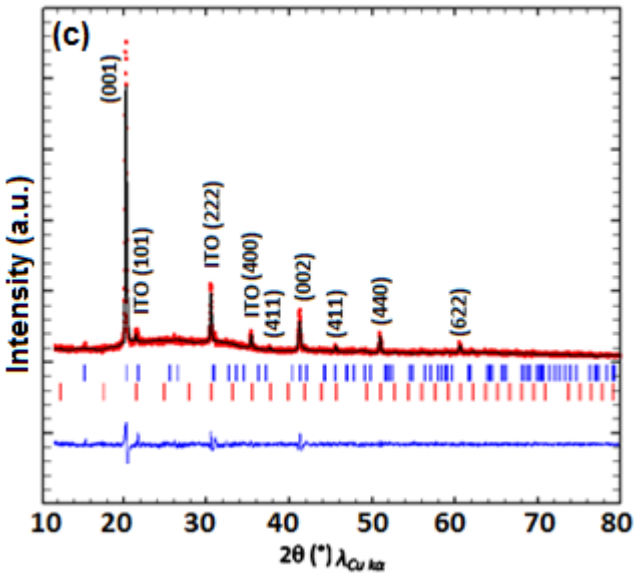

FIGURE 4. SEM images of V_2O_3 film (a) and V_2O_5 film (b); full-pattern matching using an anisotropic peak profile for V_2O_5 film (c) deposited by Doctor-Blade method.

II.3. Electrochromic properties of V_2O_3 and V_2O_5 films

The electrochemical stability is one of the key parameters to be taken into account when aiming at applications. Electrochemical properties of V_2O_3 and V_2O_5 films coated on ITO / glass substrate were evaluated for comparison by cyclic voltammograms (CV) followed by *ex-situ* optical measurements. As discussed below, the repetitive cycling of V_2O_3 and V_2O_5 thick film in ionic liquid (LiTFSI-EMITFSI) at a scan rate of 20 mV/s shows good cyclability and stability up to 500 cycles. It should be emphasized that to our knowledge such cyclability of V_2O_3 thick films has not been reported in the literature yet.

Figure 5a displays the 1st, 5th and 500th CV of V_2O_3 film cycled in ITO/V_2O_3/LiTFSI-EMITFSI/Pt vs SCE cells started in oxidation. The small capacity of the first oxidation is rapidly followed by a reversible cycling. Upon reduction, the voltammograms show a large current wave, constituted of two main peaks located at 0.45 V and -0.47 V while in oxidation, two main peaks located at 0.51 V and 0.93 V are visible. The reversibility of the process is illustrated by a Coulombic efficiency defined as a Q_{red}/Q_{ox} ratio keeping close to 100% (**Figure S2a**), while a slight increase in capacity is observed with cycling. The colors reached by the films at different voltages measured by diffuse reflectance in the range of 400 - 800 nm are presented in **Figure 5b**. The V_2O_3 films switch reversibly in-between a reduced blue state (-0.9 V) and an oxidized-orange state (+1.9 V) associated with reflectance values less than 5% and of 35% at 600 nm, respectively, leading to an optical reflectance modulation, ΔR, of about 30%.

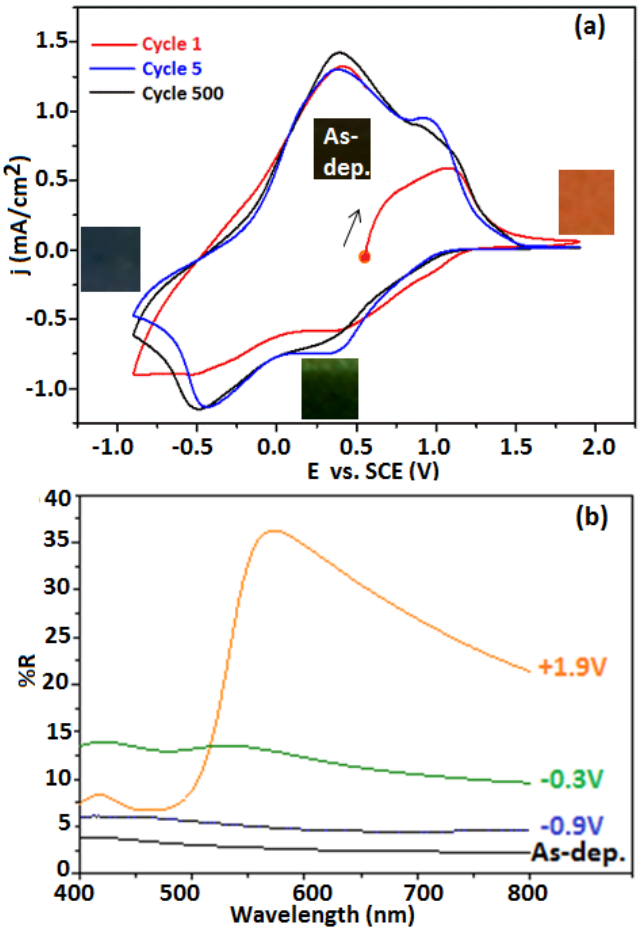

FIGURE 5. Cyclic voltammograms for V_2O_3 film cycled in ITO/V_2O_3/LiTFSI-EMITFSI/Pt vs SCE (a). *ex-situ* diffuse reflectance spectra of the V_2O_3 films at various potentials at 50th cycle : black initial state (as-deposited), oxidized orange state (+1.9V), reduced green state (-0.3V) and more reduced blue state (-0.9V) (b).

In CIE colorimetric space, the color is represented by three parameters, the luminance axis (L*) and two hue axes (a*) and (b*), which can be used to define and compare quantitatively the colors. The relative luminance (L*), the hue (a*) and (b*) values of V_2O_3 films in different states were calculated from the reflectance spectra. For the light blue-reduced state (at −0.9 V), the L*a*b* parameters are 26, -15, and -6, respectively, while for the bright orange-oxidized state (at +1.9 V) the L*a*b* parameters are 68, 11 and 56, respectively. The contrast $\Delta E^* = [(L^*_2 - L^*_1)^2 + (a^*_2 - a^*_1)^2 + (b^*_2 - b^*_1)^2]^{1/2}$ is of 79.

The repetitive cycling of V_2O_5 films using similar conditions shows also good cyclability and stability in terms of capacity up to 500 cycles (**Figure 6a**). CVs of V_2O_5 film cycled in ITO/V_2O_5/LiTFSI-EMITFSI/Pt vs SCE cells exhibit a large redox current wave constituted of different convoluted peaks, during both the positive and cathodic scans, however slightly shifted to higher potential values as compared to the ones of

V_2O_3. Furthermore, as for V_2O_3 films, and in agreement with a clear reversible process, the charges deduced from V_2O_5 cyclic

voltammetric measurements in reduction and in oxidation are equal (Q_{red}/Q_{ox}=99%) whatever the cycle number. Upon cycling the capacity significantly increases, of about 10 % in between the very first cycles and the 500th cycle (**Figure S2b**). In respect to the optical behavior, the lithium insertion/ deinsertion process is accompanied by a clear three-step electrochromism, deep blue ⇄ green ⇄orange. The V_2O_5 films switch reversibly in-between a reduced blue state (-0.9 V) and an oxidized-orange state (+1.9 V) associated with reflectance values of about 5% and 55% at 600 nm, respectively, leading to an optical reflectance modulation, ΔR, of about 50% (**Figure 6b**). For the blue, reduced state (at −0.9 V), the calculated L*a*b* parameters are 31, -14, and -9, respectively, while for the orange, oxidized state (at +1.9 V) the L*a*b* parameters are 71, 12 and 48, respectively. The contrast ΔE* is of 74. Interestingly, if similar ΔE* contrast values, of about 75 to 80 % are recorded for both oxides, the higher electrochemical capacity associated with this orange to blue transition for the V_2O_3 thick film as compared to the V_2O_5 one emphasized its good EC properties. Commonly evaluated by the color efficiency, CE, for transmisttive systems (i.e. CE = 1/Q log (T_b/T_c) where Q is the electrochemical capacity, Tb and Tc the transmittance in the bleached and colored state). In the case of thick films, the modulation of ΔE* vs Q may be indeed considered as a criteria of merit in favor of V_2O_3. In addition, the evaluation of the switching times from chronoamperometry measurements confirms the slightly higher properties of V_2O_3. Both oxides exhibit switching times of few seconds in between orange (+ 1.9 V) to blue (- 0.9 V) colors, namely 7s (oxidized orange) and 5s (reduced blue) for V_2O_3 and 9s (oxidized orange) 6s (reduced blue) for V_2O_5.

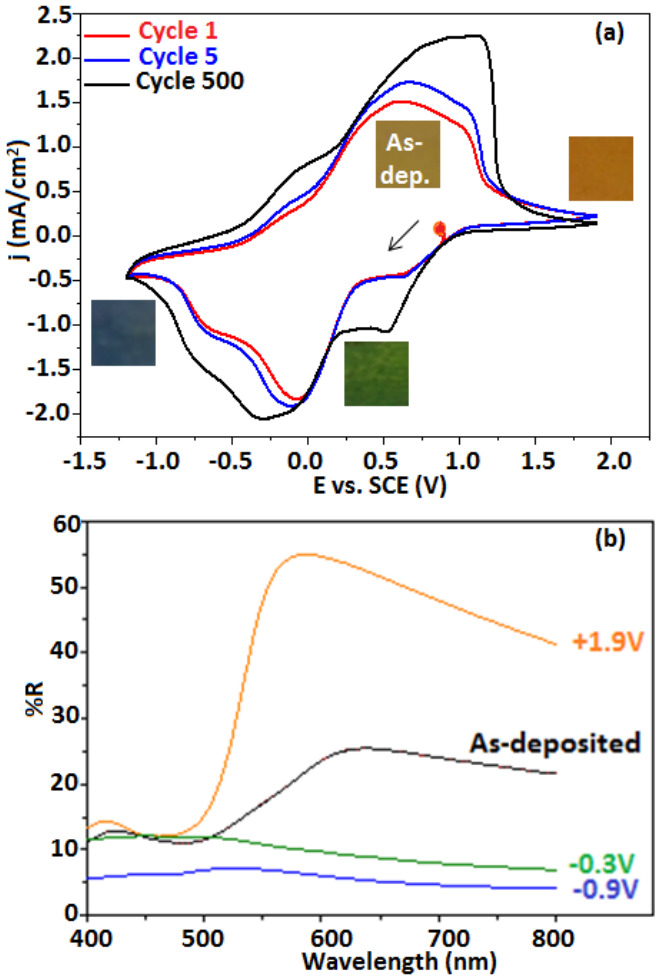

FIGURE 6. Cyclic voltammograms for V_2O_5 film cycled in ITO/V_2O_5/LiTFSI-EMITFSI/Pt vs SCE (a). *ex situ* diffuse reflectance spectra of the V_2O_5 films at various potentials at 50th cycle : initial state (as-deposited), oxidized orange state (+1.9V), reduced green state (-0.3V) and more reduced blue state (-0.9V) (b).

The memory effect, namely persistence of the colored state after the voltage being cut, is a key characteristic of electrochromic materials. In this work, both oxides show good memory effect after long times (30 days). All the films in different states (blue and orange) for both oxides were exposed in air at room temperature, and the stability of the films was tested after 30 days with no electrical voltage applied. To illustrate this stability, the L*a*b parameters for blue-reduced state (-0.9V) and orange oxidized state (+1.9V) in initial state and after 30 days were determined and are summarized in **Table S1** and **Table S2**. The analysis of the L*a*b parameters for both oxides at the initial state and after one month shows that there is no change in chromaticity parameters after 30 days. This demonstrates that V_2O_3 and V_2O_5 films possess great electrochromic color memory properties with excellent color stability at the oxidized/reduced state. Their good electrochromic color memory properties may be ascribed to the intrinsic stability and their porosity of Doctor Blading V_2O_3 and V_2O_5 films that help the electrolyte ions insertion/deinsertion

into the film to stabilize the reduced and oxidized state by Coulomb force.

The close EC behavior for both V_2O_3 and V_2O_5 films, exhibiting different morphologies, structures and compositions (i.e. different vanadium oxidation states) raises the question of the mechanism at the origin of the multichromism.

II.4. Mechanism

From what is generally accepted in V_2O_5, Li insertion and deinsertion takes place following the $V_2O_5 + xLi^+ + xe^- = Li_xV_2O_5$ reaction. Thus upon reduction the simultaneous injection of electrons and Li^+ ions into the V_2O_5 film leads to a progressive reduction of pentavalent vanadium (V^{5+}) to its lower valence state (V^{4+}) and eventually to (V^{3+}) [34] . In oxidation, the extraction of electrons and Li^+ ions from $Li_xV_2O_5$ film leads to the oxidation of lower valence vanadium (V^{4+} or V^{3+}) to its pentavalent state (V^{5+}).

The number of exchanged electrons (x) involved during each coloration/bleaching process was estimated using the following equation:[13] $Q = F*nV_2O_5*x$, where Q is the electrochemical capacity, F = 96500 C, and n is number of moles, assuming a density of 75 %. The x values calculated from V_2O_5 films is about 1.1. The number of exchanged electrons remains much lower than to the expected one if V^{5+} ions are fully reduced to V^{4+} or even V^{3+} ions.

The electrochemical behaviors of V_2O_5 and V_2O_3 films do not appear as different as it could be expected. The oxidation of V_2O_3 during the first half cycle can only be explained by oxygen anion sources. Nonetheless, the electrochromic behavior of V_2O_3, on the point of view of the change of colorations, is similar to other reports of other vanadium oxides with a three-step mechanism implying a blue to green color first change and then a green to orange color change (in oxidation scan).

The multi-step electrochromism from orange to green and green to blue, during the reduction of V_2O_5 films (with reverse phenomenon during oxidation) was previously observed by several authors.[34-37] It can be associated, as we proposed here, to a double oxidation number change (V^{5+} to V^{4+} and then V^{4+} to V^{3+}). In this way, Tong et al. [34] recently ascribed the color change to olive green to the presence of V^{3+} ions, associating the multiple colors in V_2O_5 to the presence of V^{3+}/V^{4+} and V^{5+}. Such observations well agree with the color of V^{3+}, V^{4+}, and V^{5+} in aqueous solutions: i.e., in an octahedral ligand field with aqua ligands. In the meantime, current investigations in our group on V_2O_5 thin films grown by RF sputtering confirm similar color changes of orange to green and green to blue upon cycling while only 1.5 Li are being exchanged with the single presence of V^{5+} and V^{4+}. In addition, similar multicolor electrochromism has been detected on amorphous VO_x films, with x between 1.5 and 2. Nonetheless some authors [38-40] have shown that the occurrence of a single V^{5+}/V^{4+} redox couple, can explain the green intermediate coloration by a potential range where the vanadium ions with the two oxidation numbers coexist with a well-defined ratio. Also, the electrochemical capacities we have measured, close to 1 electron only per cycle, tend to show that (i) a redox process with only oxidation numbers involving a change of only one unit occurs, or (ii) only a fraction of about 25% of the film is submitted to the redox process. To study, in our case, the oxidation number really implied in the color changes observed in both V_2O_3 and V_2O_5 films, *i.e* to investigate what are the different amount mixtures of V^{5+}, V^{4+}, and V^{3+} ions, during cycling, *ex-situ* XPS spectroscopy, for different applied voltages, was performed. The $V2p_{3/2}$ core peak spectra of the film in different potential states corresponding to the distinct colorations: for the as-prepared films, the orange state (oxidized state after 50 cycles), the green (intermediate state after 50 cycles) and the blue one (reduced state after 50 cycles), reached during electrochromic recording were analyzed (**Figures 7 and 8**), and the corresponding fitting results are shown in **Table 2**, for both V_2O_3 and V_2O_5 films.

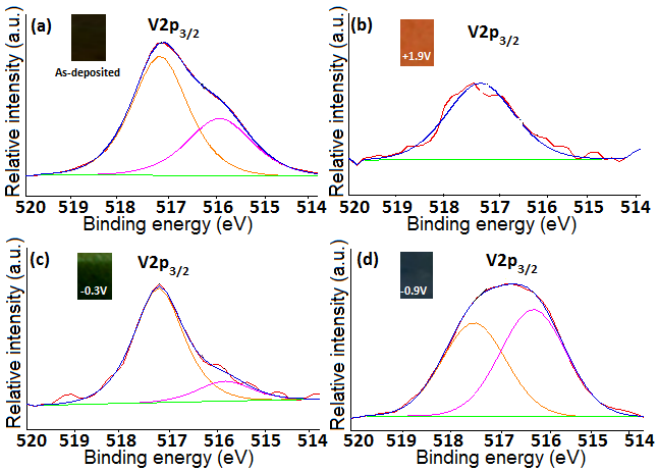

FIGURE 7. *ex-situ* XPS of V_2O_3 film before cycling (a) and after 50 cycles at oxidized state (b) reduced green state (c) and reduced blue state (d).

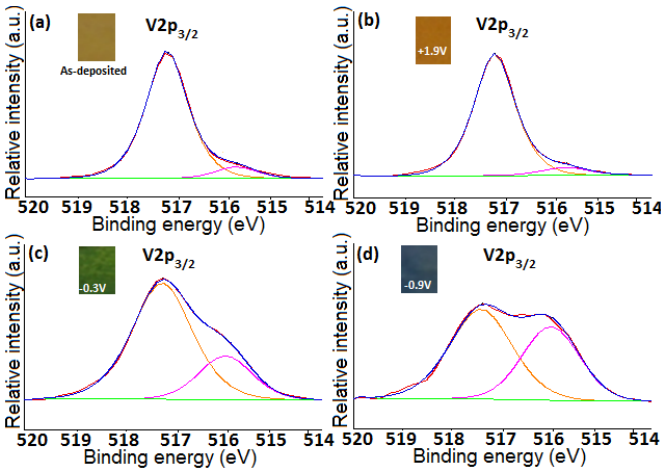

FIGURE 8. *ex situ* XPS of V_2O_5 film before cycling (a) and after 50 cycles at oxidized state (b) reduced green state (c) and reduced blue state (d).

In the potential range from +1.9V to -0.9 V, only two $V2p_{3/2}$ core peaks are identified. The orange coloration being associated with the occurrence of a very main peak near 517.5 eV, this peak can be without any ambiguities ascribed to the V^{5+} ion. [41] The second peak centered on 516 eV is, based on literature on the previous VO_x measurements, ascribed to the V^{4+} ions.[42] But, this last attribution can be contested and possibly, this peak is the convolution of the signals characteristic of both V^{3+} and V^{4+} ions. Indeed, it can be noted

that none occurrence of a distinguishable V^{3+} peak for the V_2O_3 as-prepared film is surprising. On the other hand, and interestingly, V^{4+} ions which are detected in the as-prepared film may be derived from the partial dissolution of the V_2O_5 film which was strongly suggested by the observation of a change of the crystallite morphology between the film's crystallites and the powder ones, as previously discussed. The existence of V^{4+} in the as-prepared film also explains the observed "brownish" coloration of the as-prepared film in comparison with the brilliant orange color reached in oxidative regime.

Anyway, it can be supposed that the oxidation numbers measured from XPS spectroscopy are not fully representative of the oxidation numbers in the film's bulk. Surface redox processes may occurr before the analysis. So, the attribution of the detected peak to the V^{5+} and V^{4+} ions as representative of our film composition cannot be made without uncertainties.

TABLE 2. V^{5+} and V^{4+} quantification deduced from *ex-situ* XPS study after 50 cycles (100 % corresponds to normalization of the strongest contribution).

V_2O_3 films	**V^{5+}(%)**	**V^{4+}(%)**	**$R=V^{5+}/V^{4+}$**
As-deposited (Black)	100	48	2.1
Green color (-0.3V)	100	17	5.2
Blue color (-0.9V)	87	100	0.9
Orange color (+1.9V)	100	nearly 0	-
V_2O_5 films	**V^{5+}(%)**	**V^{4+}(%)**	**$R=V^{5+}/V^{4+}$**
As-deposited (Brown)	100	9	11.1
Green color (-0.3V)	100	32	3.1
Blue color (-0.9V)	100	73	1.4
Orange color (+1.9V)	100	7	13.8

Whatever, the difficulty to ascribe the different XPS core peaks to well-defined oxidation states, the evolution during cycling of the two different compositions studied and their comparison put into evidence remarkable similarities. The $R=V^{5+}/V^{4+}$ ratios evolve quite similarly versus the applied potential for both V_2O_3 and V_2O_5 films. For a green coloration at -0.3 V, the V^{5+}/V^{4+} ratio is in favor of the V^{5+} ion, but with a significant minor peak of V^{4+} signal; whereas this ratio is roughly around the unit, i.e. showing an equilibrate partition between V^{5+} and V^{4+} ions, when the blue color is obtained at -0.9 V. For the return sweep, in oxidative regime at 1.9 V, leading to an orange color, it is found that the V^{5+} ions are at the origin of nearly the whole XPS signal. From the *ex-situ* XPS analysis it seems that the multi-electrochromism showed in our V_xO_y films, whatever the starting chemical composition, is due to switches between the vanadium states +4 and +5. Especially, and without any ambiguities on this important suggestion, the oxidation of the vanadium oxide films, whatever their initial composition/structure, leads to a complete vanadium oxidation, it means that a pure V_2O_5 orange compound is reached.

To confirm the most significant result obtained by XPS, that is the complete oxidation of the vanadium species to oxidation state equal to 5 while an oxidative potential of 1.9 V is applied, starting from V_2O_5 as well as V_2O_3 film composition, X-ray analyses were performed (**Figures 9 and 10**).

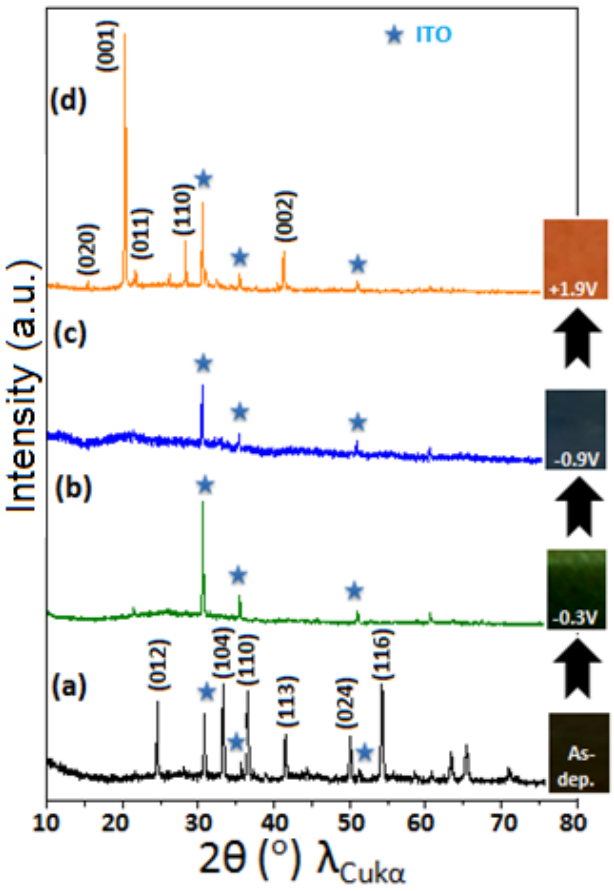

FIGURE 9. *ex-situ* Grazing incidence XRD of V_2O_3 film before cycling (a) and after 50 cycles at oxidized state (b) reduced green state (c) and reduced blue state (d).

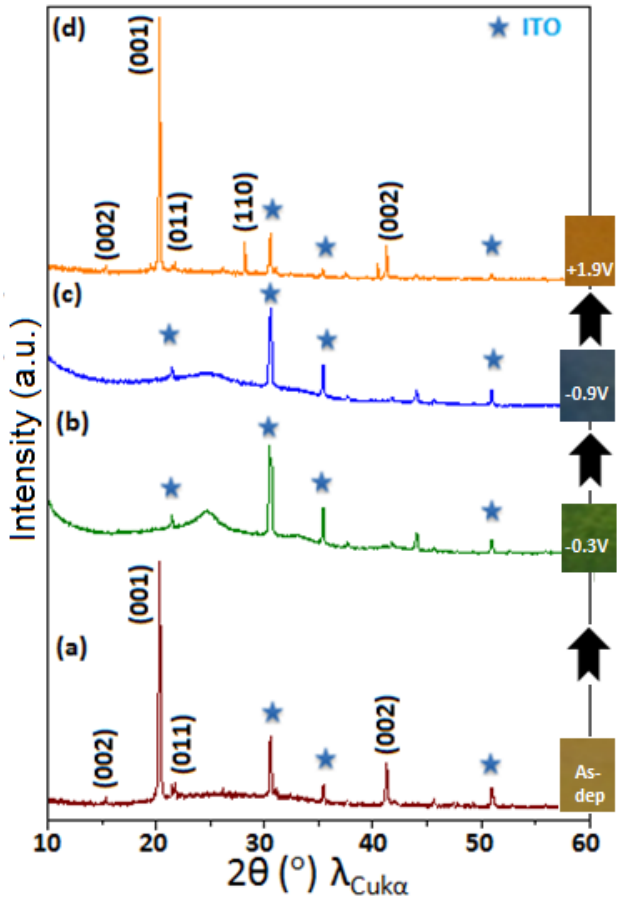

FIGURE 10. *ex-situ* Grazing Incidence XRD of V_2O_5 film before cycling (a) and after 50 cycles at oxidized state (b) reduced green state (c) and reduced blue state (d).

The X-ray patterns were recorded with the same grazing incidence (2°) on both V_2O_3 and V_2O_5 films for the four states of coloration previously discussed: black or brown, respectively (as-deposited), green (-0.3V), blue (-0.9V) and orange (+ 1.9V). The measurements were realized after 50 cycles.

In **Figure 9**, all the peaks of the as-deposited V_2O_3 with black coloration are perfectly indexed to V_2O_3 phase without any preferential orientation (**Figure 9a**); the X-ray pattern for the film and the powder (Figure 1a) can be superimposed. For the two potentials corresponding to the green and the blue colors (**Figure 9b and 9c**), one can note the absence of the characteristic peaks of any VO_x phase: the film becomes amorphous; the peaks, which are observed, are due to the ITO sub-layer. In oxidative regime (+1.9 V) (Figure 9d), leading to an orange coloration, the additional peaks observed on the X-ray pattern, besides the ITO's peaks, can be indexed as well crystallized orthorhombic V_2O_5 (SG: Pmmn).

In **Figure 10**, the X-ray patterns show that for as-deposited V_2O_5 with brownish coloration, all the peaks are perfectly indexed to V_2O_5 phase with a preferential orientation along the c-axis while for the reduction (to green and blue colors), only the peaks associated with ITO are observed. As previously, well-crystallized V_2O_5 is reformed upon oxidation.

These results are in agreement with the ones obtained by XPS; especially, V_2O_5 single phase in oxidation is confirmed. Indeed, whatever the starting composition, the X-ray pattern for the re-oxidized film after 50 cycles reveals that all peaks are identified to the vanadium pentoxide with high crystallinity. From *ex-situ* XRD analysis, it can be concluded that during cycling vanadium oxides pass through amorphous state during the reduction and that this state should be characterized by a mixture of V^{4+} and V^{5+}. During the return sweep, all the vanadium ions are fully oxidized into V^{5+} state, in agreement with the orange color. More surprisingly, the complete re-oxidation, at the end of each cycle, allows each time the recrystallization of V_2O_5. Finally, the kinetic of the phenomenon was studied on the as-prepared V_2O_3 film, comparing the X-ray pattern recorded for an applied voltage of +1.9 V, after 5 cycles and 50 cycles (**Figure S3**). This comparison shows that even after 5 cycles, V_2O_5 single phase is already obtained. However, the strong preferential orientation of the film drastically increases between the 5th and the 50th cycle. This observation confirms a reorganization of the atomic matter all along the cycling processes, and can justify the slight coulombic efficiency increase observed for the V_2O_3 starting film with the number of cycles.

III. CONCLUSION

In this study, we show a robust scenario that provides access to stoichiometry-controlled and which leads to: (i) the synthesis of two oxides V_2O_3 and V_2O_5 from a single polyol route, (ii) the demonstration for the first time of the electrochromic properties of V_2O_3, (iii) a "multi-color" electrochromic behavior very similar while one compares V_2O_3 and V_2O_5 (i.e. independently of the starting stoichiometry), which is associated with an unusual recrystallization process of V_2O_5 in oxidative regime. The latter represents a great step forward for the understanding of the electrochromic properties of vanadium oxides. Moreover, it is also a progress in solid state chemistry since a new synthesis method for obtaining well-crystallized V_2O_5 films, with a strong preferential orientation, can be proposed from the oxidation of any VO_x films.

IV. EXPERIMENTAL SECTION

A detailed description of all the experimental procedures and techniques characterization is given in the supporting information (SI).

ASSOCIATED CONTENT

Supporting Information

The Supporting Information is available free of charge on the ACS Publications website at DOI:

It contains a detailed description of all the experimental procedures and techniques of characterization including the XRD of V_2O_3 powders and film, and ITO substrate and coulombic efficiency and its evolution during cycling for V_2O_3 and V_2O_5 films cycled in ITO/V_2O_3 (V_2O_5)/LiTFSI-EMITFSI/Pt vs SCE cell. We also determine the L*a*b* parameters in the blue-reduced state and orange-oxidized state of V_2O_3 and V_2O_5 at initial state and after 30 days and also the *ex-situ* XRD of V_2O_3 film before cycling, after 5 cycles and 50 cycles in oxidized state.

AUTHOR INFORMATION

Corresponding Author

*E-mail: aline.rougier@icmcb.cnrs.fr

ORCID

Issam Mjejri: 0000-0001-5313-3198
Manuel Gaudon : 0000-0002-6918-2004
Aline Rougier: 0000-0002-1340-734X

Author Contributions

The manuscript was written through contributions of all authors. All authors have given approval to the final version of the manuscript.

Notes

The authors declare no competing financial interest.

REFERENCES

(1) Li, Z. J. ; Shao, J. Y. ; Zhong, Y. W. Near-Infrared and Two-Wavelength Electrochromism Based on Nanocrystalline TiO_2 Films Functionalized with Ruthenium-Amine Conjugated Complexes. Inorg. Chem., 2017, 56, 8538–8546.
(2) Cai, G.; Wang, J.; Lee, P. S. Next-Generation Multifunctional Electrochromic Devices. Acc. Chem. Res. 2016, 49, 1469-1476.
(3) Yang, P.; Sun, Peng.; Mai, W. Electrochromic Energy Storage Devices. Mater., Today, 2016, 19, 394.
(4) Liu, Y.; Lv, Y.; Tang, Z.; He, L.; Liu, X. Highly Stable and Flexible ITO-Free Electrochromic Films with Bi-functional Stacked MoO_3/Ag/MoO_3 Structures. Electrochim. Acta 2016, 189, 184-189.
(5) Papaefthimiou, S.; Leftheriotis, G.; Yianoulis, P. Advanced Electrochromic Devices Based on WO_3 Thin Films. Electrochim. Acta 2001, 46, 2145-2150.
(6) Bucha, V. R.; Chawla, A. K.; Rawal, S. K.. Review on Electrochromic Property for WO_3 Thin Films Using Different Deposition Techniques. Mater. Today: Proceedings 2016,3 , 1429-1437.
(7) Granqvist, C. G. Oxide electrochromics: An Introduction to Devices and Materials. Sol. Energy Mater. Sol. Cells, 2012, 99, 1-13.
(8) Dalavi, D. S.; Devan, R. S.; Patil, R. A.; Patil, R. S.; Ma, Y. R.; Sadale, S. B.; Kim, I.; Kim, J. H.; Patil, P. S. Efficient Electrochromic Performance of Nanoparticulate WO_3 Thin Films. J. Mater. Chem. C, 2013, 1, 3722–3728.
(9) Chu, C. H.; Wu, H. W.; Huang, J. L. Novel WO_3-Based Electrochromic Device for High Optical Modulation and Infrared Suppression. ieee electron device lett., 2015, 36, 256.
(10) Danine, A.; Cojocaru, L.; Faure, C.; Olivier, C.; Toupance, T.; Campet, G.; Rougier, A. Room Temperature UV Treated WO_3 Thin Films for Electrochromic Devices on Paper Substrate. Electrochim. Acta 2014, 129, 113-119.
(11) Beaujuge, P. M.; Ellinger, S.; Reynolds, J. R. The Donor–Acceptor Approach Allows a Black-to-Transmissive Switching Polymeric Electrochrome. Nat., Mater., 2008, 7, 795-799.
(12) Mjejri, I.; Doherty, C. M.; Martinez, M. R.; Drisko, G.L.; Rougier, A. Double Sided Electrochromic Device Based on Metal-Organic Frameworks. ACS Appl. Mater. Interfaces 2017, 9, 39930.
(13) Mjejri, I.; Manceriu, L.M.; Gaudon, M.; Rougier, A.; Sediri, F. Nano-Vanadium Pentoxide Films for Electrochromic Displays. Solid State Ionics 2016, 292, 8-14.
(14) Talledo, A.; Granqvist, C. G. Electrochromic Vanadium-Pentoxide-Based Films: Structural, Electrochemical, and Optical Properties. J. Appl. Phys. 1995, 77, 4655.
(15) Cogan, S.F.; Nguyen, N. M.; Perrotti, S.J.; Rauh R. D. Optical Properties of Electrochromic Vanadium Pentoxide. J. Appl. Phys. 1989, 66, 1333.
(16) Kovendhan, M.; Joseph P. D.; Manimuthu, P.; Sendilkumar, A.; Karthick, S.N.; Sambasivam, S.; Vijayarangamuthu, K.; Kim, H. J.; Choi, B. C.; Asokan, K.; Venkateswaran, C.; Mohan R. Prototype Electrochromic Device and Dye Sensitized Solar Cell using Spray Deposited Undoped and 'Li' Doped V_2O_5 Thin Film Electrodes. Curr. Appl. Physics, 2015, 15, 622-631.
(17) Lee, S.H.; Cheong, H.M.; Liu, P.; Tracy, C.E.; Pitts, J.R.; Deb, S. K. Improving the Durability of Ion Insertion Materials in a Liquid Electrolyte. Solid State Ionics 2003, 165, 81-87.
(18) Wang, B.Y.; Takahashi, K.; Lee, K.; Cao, G. Nanostructured Vanadium Oxide Electrodes for Enhanced Lithium-Ion Intercalation. Adv. Funct. Mater., 2006, 16, 1133-1144.
(19) Wang, Y.; Cao, G. Li^+-Intercalation Electrochemical/Electrochromic Properties of Vanadium Pentoxide Films by Sol Electrophoretic Deposition. Electrochim. Acta 2006, 51, 4865-4872.
(20) Yao, J.; Li, Y.; Massé, R.C.; Uchaker, E.; Cao, G. Revitalized Interest in Vanadium Pentoxide as Cathode Materials for Lithium-ion Batteries and Beyond. Energy Storage Materials, 2018, 11, 205-259.
(21) Garcia-Lobato, M. A.; Martinez, A. I.; Perry, D. L.; Castro-Roman, M.; Zarate, R. A.; Escobar-Alarcon, L. Elucidation of the Electrochromic Mechanism of Nanostructured Iron Oxides Films. Sol Energy Mater. Sol. Cells 2011, 95, 751-758.
(22) Gonçalves, A.; Resende, J.; Marques, A.C.; Pinto, J.V.; Nunes, D.; Marie, A.; Goncalves, R.; Pereira, L.; Martins, R.; Fortunato, E. Smart Optically Active VO_2 Nanostructured Layers Applied in Roof-Type Ceramic Tiles for Energy Efficiency. Sol. Energy. Mater. Sol. Cells 2016, 150, 1–9.
(23) Wu, C.; Feng, F.; Xie, Y. Design of Vanadium Oxide Structures with Controllable Electrical Properties for Energy Applications. Chem. Soc. Rev., 2013, 42, 5157-5183.
(24) Santulli, A. C.; Xu, W.; Parise, J. B.; Wu. L.; Aronson, M. C.; Zhang, F.; Nam, C. Y.; Black, C. T.; Tiano, A. L.; Wong, S. S. Synthesis and Characterization of V_2O_3 Nanorods. Phys. Chem. Chem. Phys., 2009, 11, 3718-3726.
(25) Quinzeni, I.; Ferrari, S.; Quartarone, E.; Mustarelli, P. Structural, Morphological and Electrochemical Properties of Nanocrystalline V_2O_5 Thin Films Deposited by Means of Radiofrequency Magnetron Sputtering. J. Power Sources 2011, 196, 10228–10233.

(26) Li, L.; Steinera, U.; Mahajan, S. Improved Electrochromic Performance in Inverse opal Vanadium Oxide Films. J. Mater. Chem., 2010, 20, 7131–7134.
(27) Niu, C.; Han, C.; Zhao, Y.; Tian, X.; Guo, W.; Gu, Y.; Ma, L. Synthesis and Optical Property of Size-Tunable Vanadium Oxide Nano-Dandelions. J. Nanosci. Lett. 2013, 3: 27
(28) Chu, J., Kong, Z., Lu, D., Zhang, W., Wang, X., Yu, Y., Li, S., Wang, X., Xiong, S., Ma, J. Hydrothermal Synthesis of Vanadium Oxide Nanorods and their Electrochromic Performance. Mater. Lett., 2016, 166, 179.
(29) Kamalam, M.B.R.; Balachander, B.K.; Sethuraman, K. Solvothermal Synthesis and Characterization of Reduced Graphene Oxide/ Vanadium Pentoxide Hybrid Nanostructures. Mater. Today: Proceedings, 2016, 3, 2132-2140.
(30) Berezina, O., Kirienko, D., Pergament, A., Stefanovich, G., Velichko, A., Zlomanov, V. Vanadium Oxide Thin Films and Fibers Obtained by Acetylacetonate Sol-Gel Method. Thin Solid Films, 2015, 574, 15.
(31) Kawashima, T., Abe, D., Washio, K. Investigation on a Source of Dominant Donor in Vanadium-Doped ZnO Films Grown by Reactive RF Magnetron Sputtering. Mater. Sci. Semicond. Process., 2017, 70, 213-218.
(32) Huotari, J., Bjorklund, R., Lappalainen, J., Spetz, A. L., Pulsed Laser Deposited Nanostructured Vanadium Oxide Thin Films Characterized as Ammonia Sensors Actuator B-Chem., 2015, 217, 22-29.
(33) Mjejri, I.; Rougier, A.; Gaudon, M. Low-Cost and Facile Synthesis of the Vanadium Oxides V_2O_3, VO_2, and V_2O_5 and Their Magnetic, Thermochromic and Electrochromic Properties. Inorg. Chem. 2017, 56, 1734-1741.
(34) Tong, Z.; Zhang, X.; Lv, H.; Li, N.; Qu, H.; Zhao, J.; Li, Y.; Liu, X.Y. From Amorphous Macroporous Film to 3D Crystalline Nanorod Architecture: A New Approach to Obtain High-Performance V_2O_5 Electrochromism. Adv. Mater. Interfaces 2015, 2, 1500230.
(35) Tong, Z.; Lv, H.; Zhang, X.; Yang, H.; Tian, Y.; Li, N.; Zhao, J.; Li, Y. Novel Morphology Changes From 3D Ordered Macroporous Structure to V_2O_5 Nanofiber Grassland and its Application in Electrochromism. Scientific Reports 2015, 5, 16864.
(36) Tong, Z.; Hao, J.; Zhang, K.; Zhao, J.; Su, B. L.; Li, Y. Improved Electrochromic Performance and Lithium Diffusion Coefficient in Three-Dimensionally Ordered Macroporous V_2O_5 Films. J. Mater. Chem. C, 2014, 2, 3651-3658.
(37) Lu, Y.R.; Wu, T.Z.; Chen, C.L.; Wei, D.H.; Chen, J.L.; Chou, W.C.; Dong, C.L. Mechanism of Electrochemical Deposition and Coloration of Electrochromic V_2O_5 Nano Thin Films: an In Situ X-Ray Spectroscopy Study. Nanoscale Res. Lett., 2015, 10, 387.
(38) Livage, J. Optical and Electrical Properties of Vanadium Oxides Synthesized From Alkoxides. Coord. Chem. Rev., 1999, 190–192, 391–403.
(39) Alsawafta, M.; Almoabadi, A.; Badilescu, S.; Truong ,V.V. Improved Electrochromic Properties of Vanadium Pentoxide Nanorods Prepared by Thermal Treatment of Sol-Gel Dip-Coated Thin Films. J .Electrochem. Soc., 2015, 162, H466-H472.
(40) Costa, C.; Pinheiro, C.; Henriques, I.; Laia, C.A.T. Electrochromic Properties of Inkjet Printed Vanadium Oxide Gel on Flexible Polyethylene Terephthalate/Indium Tin Oxide Electrodes. ACS Appl. Mater. Interfaces 2012, 4, 5266−5275.
(41) Chalker, C.J.; An, H.; Zavala, J.; Parija, A.; Banerjee, S.; Lutkenhaus, J. L.; Batteas, J.D. Fabrication and Electrochemical Performance of Structured Mesoscale Open Shell V_2O_5 Networks. Langmuir 2017, 33, 5975−5981.
(42) Xiong, C.; Aliev, A.E.; Gnade, B.; Balkus, K. J.; Jr. Fabrication of Silver Vanadium Oxide and V_2O_5 Nanowires for Electrochromics. Acs Nano, 2, 2008, 293-301.

TOC

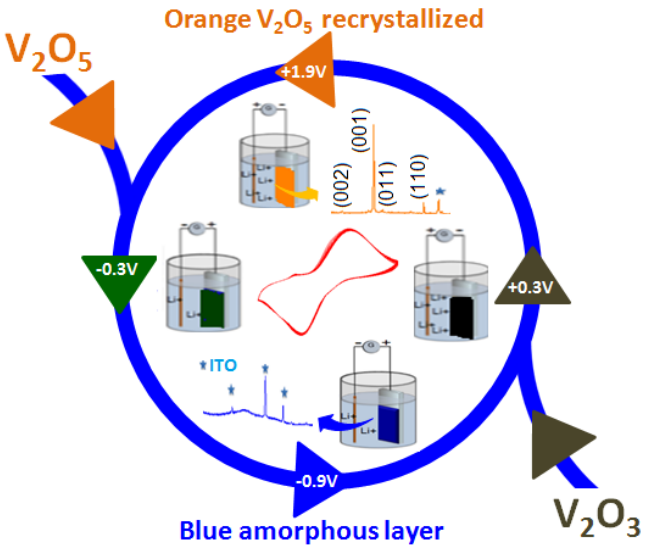
Orange V_2O_5 recrystallized
V_2O_5
+1.9V
(001)
(002)
(011)
(110)
-0.3V
+0.3V
ITO
-0.9V
Blue amorphous layer
V_2O_3